Rhamnolipid Biosurfactant and Soy Protein Act as Effective Stabilizers in the Aggregation and Transport of Palladium-Doped Zerovalent Iron Nanoparticles in Saturated Porous Media

ARTICLE *in* ENVIRONMENTAL SCIENCE & TECHNOLOGY · NOVEMBER 2013

Impact Factor: 5.33 · DOI: 10.1021/es402619v · Source: PubMed

3 AUTHORS, INCLUDING:

Mohan Basnet
McGill University
8 PUBLICATIONS **80** CITATIONS
SEE PROFILE

Nathalie Tufenkji
McGill University
122 PUBLICATIONS **3,625** CITATIONS
SEE PROFILE

Environmental Science & Technology

Article

pubs.acs.org/est

Rhamnolipid Biosurfactant and Soy Protein Act as Effective Stabilizers in the Aggregation and Transport of Palladium-Doped Zerovalent Iron Nanoparticles in Saturated Porous Media

Mohan Basnet,[†] Subhasis Ghoshal,[‡] and Nathalie Tufenkji*,[†]

[†]Department of Chemical Engineering, McGill University, Montreal, Quebec H3A 2B2, Canada

[‡]Department of Civil Engineering, McGill University, Montreal, Quebec H3A 2K6, Canada

Supporting Information

ABSTRACT: Palladium-doped nanosized zerovalent iron (Pd-NZVI) particles can contribute to the transformation of chlorinated solvents and various other contaminants into innocuous products. To make Pd-NZVI an effective in situ subsurface remediation agent, these particles need to migrate through a targeted contaminated area. However, previous studies have reported very limited mobility of these particles in the groundwater environment and attributed it to rapid aggregation and subsequent pore plugging. In this study, we systematically investigated the influence of selected natural and nontoxic organic macromolecules (carboxymethyl cellulose, rhamnolipid biosurfactants, and soy protein) on the aggregation and transport behavior of bare and coated Pd-NZVI. Aggregation behavior was investigated using dynamic light scattering by monitoring the evolution of hydrodynamic diameter as a function of time, whereas transport behavior was investigated by conducting water-saturated sand-packed column experiments. While bare Pd-NZVI is prone to rapid aggregation, we observed good colloidal stability and concurrent enhanced transport of Pd-NZVI coated with carboxymethyl cellulose, rhamnolipid biosurfactants, and soy protein. Each surface modifier performed well at lower ionic strength (IS) (10 mM $NaHCO_3$), and one of the rhamnolipid surface modifiers (JBR215) significantly enhanced transport of 150 mg/L Pd-NZVI at concentrations as low as 10 mg/L total organic carbon. However, an increase in the solution IS induced significant Pd-NZVI aggregation with a simultaneous decrease in the transport potential in accordance with the DLVO (Derjaguin, Landau, Verwey, and Overbeek) theory of colloidal stability. Nonetheless, at the highest IS (300 mM $NaHCO_3$) investigated, the mobility of rhamnolipid-coated Pd-NZVI is significantly higher than that of Pd-NZVI coated with the other surface modifiers, suggesting that biosurfactants may be the most suitable surface modifiers in field application. Overall, this study emphasizes how stabilization of Pd-NZVI with natural macromolecules such as rhamnolipids can improve the transport potential of these reactive nanoparticles in subsurface remediation applications at concentrations significantly lower than those of other commonly used polymers.

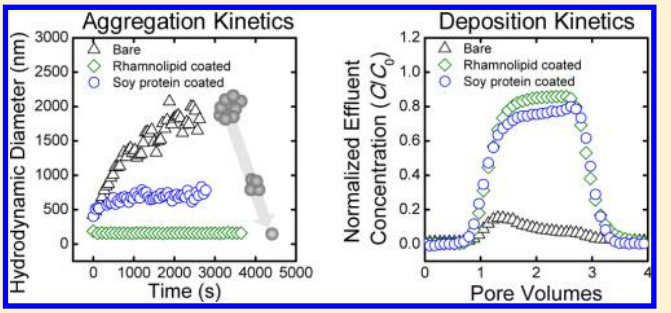

INTRODUCTION

Nanosized zerovalent iron (NZVI) and bimetallic, e.g., palladium-doped, NZVI have been shown to be promising engineered nanomaterials for the in situ subsurface remediation of various contaminants, including chlorinated hydrocarbons, heavy metals (mercury and arsenic), and others.[1−3] The success of this remediation technology largely depends on how efficiently the NZVI travels in the natural subsurface environment. However, previous studies have reported very limited mobility of bare (uncoated) NZVI and attributed this to rapid particle aggregation and subsequent entrapment in the granular porous matrixes.[4,5] Moreover, because the reactivity of NZVI is associated with its enhanced specific surface area, an increase in particle size due to aggregation could significantly reduce its reactivity toward the contaminant.[2,6]

One strategy to reduce aggregation and thereby render the reactive particles more mobile in the groundwater environment is to modify the surface of the bare particle with polymers.[7] For NZVI particles, the surface modification (or coating) reduces particle aggregation as it counters the attractive (magnetic and van der Waals) interparticle forces with the repulsive steric and/or electrostatic forces depending on the type of surface modifiers selected. Such surface modification is also expected to improve particle transport with the introduction of electrostatic and/or steric forces, limiting the deposition of NZVI onto the collector (aquifer grain) surface.[8] The stability of nanoparticles in the groundwater environment is generally assessed in the context of DLVO (Derjaguin, Landau, Verwey, and Overbeek) theory.[9,10] According to classical DLVO theory, the total

Received: June 13, 2013
Revised: October 18, 2013
Accepted: October 28, 2013

dx.doi.org/10.1021/es402619v | Environ. Sci. Technol. XXXX, XXX, XXX−XXX

interaction energy (or force) between two surfaces (particle−particle or particle−collector in the case of aggregation and deposition, respectively) can be calculated as the sum of (i) van der Waals (VDW) and (ii) electrical double-layer (EDL) interactions.[11] However, non-DLVO forces (e.g., steric interaction and magnetic forces for iron-based nanoparticles) can also play an important role, and it has been proposed to extend the DLVO theory with the addition of those forces.[12]

Several earlier studies have proposed the use of various polymers, polyelectrolytes, and surfactants to stabilize NZVI suspensions[3,4,13−20] and have observed reduced nanoparticle aggregation[13−16] or improved transport in granular porous media.[3,4,17−20] A significant quantity of NZVI-associated surface modifier (or stabilizing agent) is expected to be injected in practical applications. Thus, there is a need to identify innocuous, readily available, renewable material-based NZVI-stabilizing agents.

Various surface modifiers, including carboxymethyl cellulose (CMC),[3,14,15,19,21] poly(acrylic acid) (PAA),[15,19,22] polyaspartate (PAP),[14] poly(styrenesulfonate) (PSS),[14,15] surfactant sodium dodecylbenzenesulfonate (SDBS),[18,23] triblock copolymer,[18,23] amphiphilic graft copolymers (APGCs),[16] polyacrylamide (PAM),[15] and surfactant Tween 20,[24] have been proposed to improve nanoiron particle stability. Phenrat et al.[14] compared the stabilizing efficiency of three polyelectrolytes (CMC, PSS, and PAP) and found that PSS is more effective than PAP and CMC in stabilizing NZVI and attributed its performance to increased mass and thickness of the adsorbed PSS layer. In another study, Cirtiu et al.[15] compared the stabilizing efficiency of four types of polymers (PSS, CMC, PAA, PAM) using both pregrafting and postgrafting surface modification approaches. That study demonstrated that the colloidal stabilization by pregrafted CMC was more efficient than that of other pre- or postgrafted polymers and attributed this to a strong chemical bond between the carboxylate groups of CMC and the iron oxide surface of NZVI. It should be noted that although coated surface modifiers reduce aggregation, there is still some residual aggregation.[14,21,25] Raychoudhury et al.[25] demonstrated that such residual aggregation can lead to time-dependent particle size distributions (PSDs) and deposition rate coefficients, even with polymer-coated NZVI. The use of food-grade surface modifiers such as guar gum,[13,17] xanthan gum,[20] starch,[26] and soy protein[27] has also been demonstrated in recent studies.

We have previously shown that the presence of environmental macromolecules (rhamnolipid and Suwannee River fulvic acid) can influence the deposition kinetics of CMC-NZVI whereby the lowest nanoparticle deposition rates onto a QCM-D (quartz crystal microbalance with energy dissipation) silica crystal were observed in the presence of rhamnolipid.[21] Furthermore, rhamnolipid biosurfactants enhance the solubilization and emulsification of subsurface organic contaminants.[28] The heightened aqueous solubility makes the contaminant more readily available to Pd-NZVI injected for remediation. An example of rhamnolipid application in environmental remediation includes washing the contaminated soils to remove hydrocarbons and heavy metals. Fan et al.[29] used rhamnolipid to increase the solubility of PCB in contaminated soil remediated by xanthan gum-stabilized nanosized Pd/Fe. Lai et al.[30] showed enhanced removal of total petroleum hydrocarbons from a contaminated soil while using rhamnolipid biosurfactant in comparison with synthetic surfactants. In another study, Juwarkar et al.[31] demonstrated the potential of using rhamnolipid biosurfactant to remove heavy metals (cadmium and lead) from contaminated soils.

Earlier studies have examined the role of surface modifiers on the mobility of NZVI. Saleh et al.[4] demonstrated improved NZVI mobility in saturated quartz sand when the particles were coated with SDBS and a triblock copolymer. Johnson et al.[32] observed enhanced bare NZVI mobility when the particle was suspended in the presence of natural organic matter. Likewise, Tiraferri and Sethi[17] proposed guar gum as a stabilizing agent to improve NZVI mobility in sand. In another study, Raychoudhury et al.[19] showed that CMC- and PAA-coated NZVI exhibits improved transport potential over a range of porewater velocities and particle concentrations.

Although NZVI has been widely proposed as an effective remediation agent, the reactivity of NZVI can be considerably improved in the presence of a noble-metal catalyst such as palladium (Pd).[33] The presence of Pd promotes the production of reactive H species, which leads to higher reactivity.[34] The bimetallic Pd-doped NZVI (Pd-NZVI) may be preferred in a heavily contaminated site and/or in a site where rapid remediation is desired. However, few studies have examined the potential stabilizing efficiency of environmentally benign molecules for the more reactive Pd-NZVI.[3,35]

The aim of this study is to systematically investigate the effectiveness of CMC, rhamnolipid biosurfactants, and soy protein as Pd-NZVI-stabilizing agents for improved transport and minimal aggregation in model groundwater environments. These stabilizers were chosen on the basis of their environmentally friendly nature (biodegradable and nontoxic) and commercial availability for field-scale application. The stabilizing efficiency of the selected surface modifiers was investigated by measuring nanoparticle aggregation kinetics over a broad range of environmentally relevant groundwater ionic strengths (ISs). The transport potential was also examined by performing laboratory-scale quartz sand-packed column experiments.

MATERIALS AND METHODS

Pd-NZVI Stabilizing Agents. Six types of surface modifiers were tested to stabilize the bare Pd-NZVI particles: (i) sodium CMC (Sigma), (ii) rhamnolipid JBR215 purchased from Jeneil Biosurfactant Co. (Saukville, WI), (iii) rhamnolipid R95 purchased from AGAE Technologies, LLC (Corvallis, OR), (iv) soybean flour (SF) (Sigma), (v) soy protein (SP) isolate (Bob's Red Mill Natural Foods, Milwaukie, OR) and, (vi) soy milk (SM) (Earth's Own Food Company Inc., Vancouver, Canada). Both SP and SM were purchased from local stores. On the basis of the information the vendors provided, R95 rhamnolipid is more pure than JBR215 rhamnolipid. To experimentally verify this, the air−water interfacial tension of rhamnolipid solutions was measured at different concentrations (see the Supporting Information, Figure S1). The significantly lower interfacial tension of R95 rhamnolipid than JBR215 rhamnolipid is an indication of the higher purity of the former. All these surface modifiers are anionic with carboxyl functional groups as a source of the surface charge, and additional details on the surface modifiers are presented in Tabel S1, Supporting Information. The four stabilizers (CMC, R95, SF, and SP) were received as dry powders, whereas JBR215 and SM were received as solutions. Stock solutions were prepared by dissolving dry surface modifiers in deionized (DI) water overnight. The stock solutions were then stored at 4 °C in the dark until further use. The total organic carbon (TOC) content of each surface modifier solution was determined using a TOC

dx.doi.org/10.1021/es402619v | Environ. Sci. Technol. XXXX, XXX, XXX−XXX

analyzer (Shimadzu Corp.). For all experiments (characterization, aggregation, and transport), the concentration of surface modifiers in the suspensions was 100 mg/L TOC. The corresponding mass concentrations (g/L) were 0.30 (CMC), 0.17 (R95 and JBR215 rhamnolipid), 0.29 (SF), 0.23 (SP), and 0.27 (SM).

Nanoparticle Suspensions. A stock slurry of bare NZVI was obtained from Golder Associates Inc. (Montreal, Canada). To avoid further oxidation due to reaction with water, the slurry was vacuum-dried and stored in an inert environment (N_2-purged chamber). An NZVI stock suspension (10 g/L or 6.6 g of Fe/L) was prepared by suspending the dried mass in ultrapure N_2-purged DI followed by probe ultrasonication (Misonix sonicator, S-4000) for 20 min. The NZVI surface was doped with Pd according to the method described by Zhang[2] by adding an ethanol solution of palladium acetate (Sigma) to a well-dispersed (ultrasonicated) suspension of bare NZVI. The ratio of palladium acetate to NZVI mass was 0.01 (w/w). For each experiment, the stock suspension of 10 g/L bare palladium-doped NZVI (hereafter referred to as Pd-NZVI) was diluted in deoxygenated (N_2-purged) DI, ultrasonicated for 10 min, subsequently mixed with the surface modifiers, and equilibrated overnight (~20 h) at room temperature (~22 °C) using an end-over-end rotator. During equilibration, the Pd-NZVI and surface modifier concentrations were 0.6 g/L and 0.4 g/L TOC, respectively. Finally, the suspension was further diluted in N_2-purged DI water, yielding a Pd-NZVI suspension of 0.15 g/L and a surface modifier concentration of 0.1 g/L TOC. The solution IS was adjusted by adding $NaHCO_3$, and the pH was adjusted to 7.7 by addition of HCl. The same sample preparation method was employed for all the experiments (characterization, aggregation, and column experiments), and the initial particle number concentration in all the experiments was kept constant (at 2.4×10^{10} particles/mL, determined by considering the average initial dynamic light scattering (DLS)-measured particle size and assuming a spherical particle). The solution depletion method was employed to determine the adsorbed surface modifier concentration on the Pd-NZVI surface; additional details of the adsorption experiments are presented in the Supporting Information.

Nanoparticle Characterization. The particle hydrodynamic diameter and electrophoretic mobility (EPM) were determined using DLS and laser Doppler electrophoresis (ZetaSizer Nano ZS, Malvern). The nominal size and shape of the dried nanoparticles were determined using transmission electron microscopy (TEM) by obtaining high-resolution images. Details of the TEM methodology are presented in the Supporting Information.

Pd-NZVI Aggregation Kinetics. DLS (Zetasizer Nano ZS, Malvern) was used to monitor the evolution of the Pd-NZVI hydrodynamic diameter as a function of time. In this technique, the diffusion coefficient of aggregating nanoparticles is determined from the autocorrelation function, and the hydrodynamic diameter of the aggregate is evaluated using the Stokes–Einstein equation.[11] Experiments were conducted over a broad range of solution IS (10–500 mM $NaHCO_3$). The temporal evolution of the particle hydrodynamic diameter was monitored for 50–120 min depending on the aggregation profile obtained. The aggregation rate constant (k) was determined from the initial slope of the aggregation profile. Unfavorable (or slow) aggregation occurs at lower salt concentration and in the presence of a repulsive energy barrier, whereas an increase in salt concentration generally results in an increased aggregation rate. The minimum salt concentration beyond which the aggregation rate is insensitive to the subsequent increase in solution IS is called the critical coagulation concentration (CCC), and beyond this point the aggregation rate is diffusion limited.[11] The favorable aggregation rate constant (k_{fav}) is determined by conducting the aggregation experiment at a salt concentration above the CCC.[11] The inverse stability ratio ($1/W$) or particle–particle attachment efficiency (α_{pp}) can be obtained by normalizing the unfavorable aggregation rate constant (k) with the diffusion-limited favorable aggregation rate constant (k_{fav}):[11]

$$\frac{1}{W} = \alpha_{pp} = \frac{k}{k_{fav}} \tag{1}$$

The CCC and the experimental attachment efficiency (α_{pp}) can be related by[36]

$$\alpha_{pp} = \frac{1}{1 + \left(\frac{CCC}{C_s}\right)^{\beta}} \tag{2}$$

where C_s is the molar salt concentration and β is the slope $[d[\log(\alpha_{pp})]/d[\log(C_s)]]$ in the unfavorable aggregation regime.

To corroborate the aggregation kinetics with the transport experiments, the calculated initial zero order aggregation rate constants (k) were used to predict the nanoparticle mean hydrodynamic diameter (D_h) at the column outlet:

$$D_{h,\,outlet} = D_{h,\,initial} + kr_t \tag{3}$$

where r_t is the total particle residence time (in the injection reservoir and the column) before the particle reaches the column outlet. Because the column experiments were conducted over a relatively short time, we used a linear relationship between the change in hydrodynamic diameter and time. This is in agreement with the aggregation kinetics observed.

Pd-NZVI Deposition Kinetics. Nanoparticle transport experiments were conducted using glass chromatography columns (10/20, Amersham Biosciences) with a 1.6 cm internal diameter and an 8 cm saturated packed-bed length. The granular medium was a quartz sand with a mean size of 651 μm (U.S. mesh size −25/+30) fractionated by dry sieving from a stock having a broader grain size distribution (Granusil no. 2040, Ottawa Plant, Unimin). Sand cleaning and drying procedures were similar to previously reported methods.[37] Briefly, to remove the metallic impurities, the sand was acid washed by soaking overnight in 12 M HCl followed by a DI rinse until the pH was >6. Organic impurities on the sand were removed by baking the sand for 6 h at 800 °C. The porosity of the water-saturated packed bed was 0.38 as determined gravimetrically. For transport experiments, the column was wet packed using the background electrolyte of interest (10 or 300 mM $NaHCO_3$) followed by equilibration with ~10 pore volumes (PVs) of particle-free background electrolyte of interest. Next ~2 PVs of bare or surface-modified Pd-NZVI suspensions of known concentration C_0 were injected at a flow rate of 0.9 mL/min (equivalent to a Darcy velocity of 7.5×10^{-5} m/s or a pore water velocity of 1.96×10^{-4} m/s) into the packed columns. The residence time was 6.87 min determined using a conservative tracer (10 mM KNO_3). The chosen velocity is intermediate between the injection velocity and the

Table 1. Summary of the Measured DLS Hydrodynamic Diameter and Electrophoretic Mobility for Bare and Coated Pd-NZVI Used in Transport Experiments

		initial			at column outlet			
particle/modifier	ionic strength (mM $NaHCO_3$)	d_{DLS} (nm)	PDI[a]	electrophoretic mobility [(μm·cm)/(V·s)]	d_{DLS} (nm)	PDI[a]	electrophoretic mobility [(μm·cm)/(V·s)]	predicted mean size[b] (nm)
bare	10	1370 ± 544	0.55 ± 0.05	−1.82 ± 0.01	220 ± 134	0.65 ± 0.03	−2.71 ± 0.33	2389
	300	1462 ± 112	0.60 ± 0.24	−1.50 ± 0.10	733 ± 195	0.42 ± 0.10	−1.61 ± 0.15	3214
carboxymethyl cellulose (CMC)	10	911 ± 1	0.43 ± 0.01	−4.16 ± 0.02	977 ± 187	0.47 ± 0.00	−4.07 ± 0.01	913
	300	1603 ± 399	0.34 ± 0.05	−1.69 ± 0.09	544 ± 297	0.57 ± 0.00	−1.69 ± 0.12	2145
JBR215 rhamnolipid	10	62 ± 6	0.45 ± 0.02	−3.76 ± 0.09	53 ± 48	0.37 ± 0.02	−3.70 ± 0.03	66
	300	1009 ± 10	0.32 ± 0.01	−1.72 ± 0.06	836 ± 77	0.32 ± 0.03	−1.66 ± 0.06	1281
R95 rhamnolipid	10	78 ± 6	0.28 ± 0.07	−4.46 ± 0.16	91 ± 1	0.22 ± 0.05	−4.43 ± 0.30	78
	300	1044 ± 37	0.41 ± 0.03	−1.75 ± 0.01	843 ± 155	0.39 ± 0.02	−1.68 ± 0.01	1638
soy flour (SF)	10	310 ± 144	0.46 ± 0.10	−3.04 ± 0.02	349 ± 198	0.40 ± 0.02	−2.90 ± 0.04	310
	300	1001 ± 285	0.41 ± 0.02	−1.51 ± 0.06	566 ± 273	0.56 ± 0.09	−1.45 ± 0.06	1177
soy protein (SP)	10	177 ± 64	0.49 ± 0.03	−2.20 ± 0.02	210 ± 90	0.45 ± 0.03	−2.16 ± 0.08	213
	300	2272 ± 597	0.34 ± 0.12	−1.29 ± 0.03	663 ± 68	0.51 ± 0.02	−0.96 ± 0.07	2783
soy milk (SM)	10	101 ± 5	0.43 ± 0.01	−2.32 ± 0.02	123 ± 22	0.43 ± 0.06	−2.36 ± 0.02	116
	300	154 ± 25	0.71 ± 0.01	−0.99 ± 0.04	168 ± 4	0.58 ± 0.03	−1.01 ± 0.01	297

[a]PDI = polydispersity index. [b]The predicted mean aggregate size at the column outlet was determined using eq 3.

background groundwater velocity and is representative of velocity beyond the point of injection.[25] The effluent particle concentration C was monitored in real time using UV−vis spectroscopy at 508 nm.[18] In experiments with surface-modified Pd-NZVI, the same concentration of surface modifiers was maintained in the electrolyte during column equilibration, injection, and post-injection. The breakthrough behavior of an inert tracer (10 mM KNO_3) was also monitored by UV−vis spectroscopy (240 nm) prior to injection of Pd-NZVI. The results of column experiments were interpreted using classical colloid filtration theory.[38] The particle−collector attachment efficiency (α_{pc}) was calculated from particle breakthrough curves generated by plotting C/C_0 as a function of PVs injected and known experimental parameters as follows:[38]

$$\alpha_{pc} = -\frac{2}{3}\frac{d_c}{(1-\theta)L\eta_0}\ln\left(\frac{C}{C_0}\right) \quad (4)$$

where d_c is the mean collector diameter, θ is the bed porosity, L is the packed-bed length, and η_0 is the single-collector contact efficiency calculated using the Tufenkji−Elimelech equation.[39] The normalized particle concentration (C/C_0) was obtained by numerical integration of the particle breakthrough curves.

RESULTS AND DISCUSSION

Nanoparticle Electrophoretic Mobility. The magnitude of EDL interactions as particles approach one another or a collector surface in aquatic granular environments is strongly controlled by the magnitude and nature (positive or negative) of the particle surface charge. Hence, the EPM of Pd-NZVI was measured under the conditions used in deposition and aggregation kinetics experiments (Figure S2, Supporting Information; Table 1). The nanoparticles are negatively charged under all conditions investigated. Overall, for the different Pd-NZVI suspensions injected into the column, the coated particles are more negatively charged compared to the bare Pd-NZVI, implying that the selected anionic surface modifiers readily adsorb onto the Pd-NZVI surface. Independent adsorption studies were conducted to evaluate the adsorbed concentration of each surface modifier on the Pd-NZVI surface (Figure S3, Supporting Information). The results confirm the adsorption of the selected surface modifiers on the Pd-NZVI surface and show that the organic molecules have variable affinity for the nanoparticle surface. We also confirmed that the measured EPM was not an artifact due to dissolved polymer in the nanoparticle suspensions by examining the PSDs of the suspensions and confirming the presence of a single peak associated with the nanoparticles. For any given treatment, an increase in the solution IS from 10 to 300 mM generally decreases the absolute EPM due to compression of the electrical double layer (Figure S2). This effect is less important for the bare Pd-NZVI where the EPM changes from −1.8 to −1.5 (μm·cm)/(V·s) over the range of IS investigated. Overall, the bare Pd-NZVI is less negatively charged and is less sensitive to changes in the solution IS. The addition of soy products (SF, SM, and SP) generally makes the Pd-NZVI slightly more negative at the lower range of IS examined [e.g., the EPM ranges from −2.2 to −3.0 (μm·cm)/(V·s) at 10 mM IS] (Figure S2b). The magnitude of this negative charge decreases at higher solution IS and ranges from −1.5 to −0.99 (μm·cm)/(V·s) in 300 mM IS. Interestingly, the Pd-NZVI becomes much more negatively charged in the presence of CMC, JBR215, and R95 (Figure S2), with the EPM ranging from −3.8 to −4.5 (μm·cm)/(V·s) in 10 mM IS. Again, the magnitude of this negative charge decreases at higher solution IS and converges close to −1.7 (μm·cm)/(V·s) in 300 mM IS $NaHCO_3$. At 10 mM IS, R95-coated Pd-NZVI was most negatively charged [−4.5 (μm·cm)/(V·s)] followed by CMC, JBR215, SF, SM, SP, and the bare particle, respectively, whereas the variation is less significant [less than ∼1 (μm·cm)/(V·s)] at 300 mM IS. Thus, considering classic DLVO forces alone, the increased absolute charge of the surface-modified Pd-NZVI would likely contribute to increased stability of the nanoparticle suspensions.

We have previously shown[21] that the presence of CMC and selected environmental macromolecules (rhamnolipid and Suwannee River fulvic acid) can influence the surface charge of bare NZVI, making it more negatively charged over a broad range of IS (3−300 mM $NaHCO_3$). In another study, Saleh et al.[4] also reported a similar observation, whereby the surface of a triblock copolymer-, polyaspartate-, and surfactant-coated NZVI particle was more negatively charged than its bare

dx.doi.org/10.1021/es402619v | Environ. Sci. Technol. XXXX, XXX, XXX−XXX

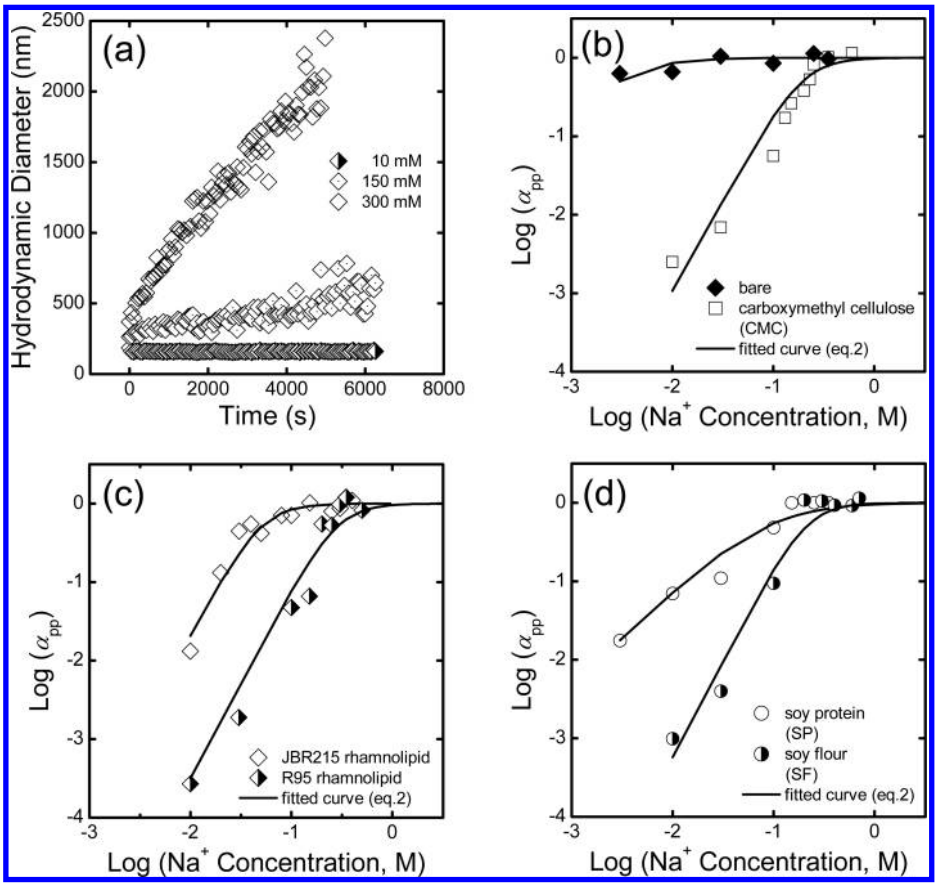

Figure 1. (a) Representative aggregation profile for R95-coated Pd-NZVI as a function of the solution IS (mM $NaHCO_3$). Particle−particle attachment efficiency (α_{pp}) for (b) bare and CMC-coated Pd-NZVI, (c) R95- and JBR215-coated Pd-NZVI, and (d) SP- and SF-coated Pd-NZVI as a function of the salt concentration (mM $NaHCO_3$). To calculate α_{pp} using eq 1, the favorable aggregation rate (k_{fav}) was determined separately for each treatment. Solid lines represent the least-squares regression of eq 2 to the experimental data.

counterpart. Those researchers reported the bare nanoparticle EPM as −2.32 (μm·cm)/(V·s) at 1 mM $NaHCO_3$ (pH 7.4), which is comparable to the EPM of the bare Pd-NZVI we measured [−1.8 (μm·cm)/(V·s)] at 10 mM $NaHCO_3$ (pH 7.7). The lower absolute EPM measured herein could be attributed to the charge-screening effect at higher IS (10 mM $NaHCO_3$) compared to the previous study at 1 mM $NaHCO_3$.[4]

Nanoparticle Sizing. Particle size is a key factor determining the fate of particle−particle interactions (in the case of nanoparticle aggregation) or particle−collector interactions (in the case of nanoparticle deposition). For nanoparticles, the likelihood of collision between two surfaces is mainly governed by Brownian diffusion. However, as the particle size increases with time (e.g., due to aggregation), other collision mechanisms (i.e., interception and sedimentation) start to become more important.[12] Although bare Pd-NZVI can be well dispersed using ultrasonication, it is prone to rapid aggregation from nanosized particles to micrometer-sized aggregates within a few minutes due to magnetic interactions.[5] Therefore, it is of interest to compare the size of Pd-NZVI both in the presence and in the absence of the selected stabilizing agents. We observe a large DLS size of the bare particle (~1.5 μm) at all the ISs investigated (Table 1). The nominal size of the primary particle, as determined by TEM, is <100 nm (Figure S4, Supporting Information).

The addition of surface modifiers decreased the extent of aggregation significantly (Table 1). At 10 mM IS, where the aggregation is minimal, the smallest hydrodynamic diameter (<100 nm) is observed for JBR215- and R95-coated particles. The DLS size is between 100 and 500 nm for the SF-, SP-, and SM-coated particles, whereas it is >500 nm for CMC-coated particles. The particle size increases with increasing solution IS as seen in the representative aggregation profile (Figure 1a). This can be attributed to charge screening and compression of the EDL at higher salt concentration. At salt concentrations beyond the CCC (e.g., 300 mM IS), the size of both bare and coated particles exceeds 1 μm (except for the SM treatment) (Table 1).

The homogeneity of the Pd-NZVI suspensions was qualitatively assessed using the polydispersity index (PDI) obtained from the DLS measurements. A PDI value of <0.1 reflects a relatively narrow monomodal particle size distribution. Because the PDI of all the suspensions was >0.1, all the suspensions employed in the transport experiments exhibited some degree of polydispersity. The largest PDI value (>0.5) was observed for bare and SM-coated particles at 300 mM IS.

Aggregation Kinetics. The aggregation behavior of bare and coated Pd-NZVI was investigated over a broad range of IS (10−500 mM $NaHCO_3$). Representative aggregation profiles (for R95-coated Pd-NZVI) are presented in Figure 1a, and representative temporal changes of the PSDs for each treatment are presented in Figures S5−S7, Supporting Information. The data in Figure 1a show that the rhamnolipid-coated Pd-NZVI is very stable at the lowest IS examined, but the particles aggregate rapidly at the highest salt concentration (300 mM). Values of the particle−particle attachment efficiency (α_{pp})

dx.doi.org/10.1021/es402619v | Environ. Sci. Technol. XXXX, XXX, XXX−XXX

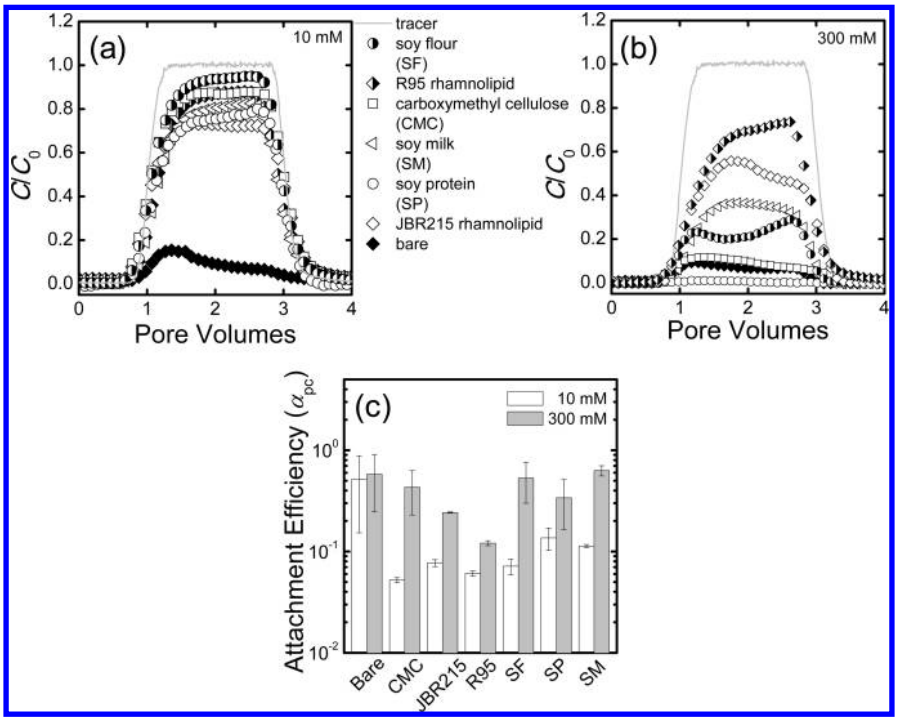

Figure 2. Measured breakthrough curves for bare and CMC-, JBR215-, R95-, SF-, SP-, and SM-coated Pd-NZVI at (a) 10 mM $NaHCO_3$ and (b) 300 mM $NaHCO_3$. The transport experiments were conducted in a clean quartz sand column (mean grain size 651 μm and porosity 0.38) with an approach velocity of 7.5×10^{-5} m/s. The breakthrough behavior of the conservative tracer (10 mM KNO_3) is also presented. (c) Particle−collector attachment efficiency (α_{pc}) for each experiment calculated using TE correlation.[39]

determined from the initial slopes of the particle aggregation profiles measured at different solution ISs are plotted in Figure 1b−d. Overall, the stability plots of the different coated Pd-NZVI follow the qualitative trend predicted by DLVO theory; namely, α_{pp} increases with increasing IS until the particle aggregation rate reaches the diffusion-limited rate ($\alpha_{pp} \approx 1$). In contrast, the bare Pd-NZVI is prone to rapid aggregation even at low IS due to strong particle−particle magnetic attraction (Figure 1b).

When Pd-NZVI is coated with CMC, rhamnolipids, or soy products, unfavorable (slow) aggregation occurs at lower salt concentrations where repulsive particle−particle interactions dominate the system. Under these conditions, the aggregation behavior is reaction limited and the particle−particle attachment efficiency is $\ll 1$ (Figure 1b−d). For example, at 10 mM IS, the value of α_{pp} for R95-coated Pd-NZVI is smallest (~0.0001), followed by those for CMC- and SF-coated Pd-NZVI (~0.001), JBR215-coated Pd-NZVI (~0.01), and, finally, SP-coated Pd-NZVI (~0.1). For the coated Pd-NZVI particles, favorable (fast) aggregation occurs only at the higher salt concentrations, where the repulsive particle−particle interactions are eliminated due to double-layer compression. At these higher solution ISs, the aggregation behavior is diffusion-limited and α_{pp} approaches 1. For CMC-coated NZVI, Raychoudhury et al.[25] reported α_{pp} = 0.0001, which is ~10 times smaller than the α_{pp} of CMC-coated Pd-NZVI measured here. This difference in α_{pp} could be attributed to the different methods used to modify the particle surface. Raychoudhury et al.[25] employed a bottom-up approach where the CMC was present in solution during the NZVI synthesis, yielding CMC strongly covalently bonded to the NZVI surface. In the study herein, the CMC is coated or post-grafted onto the Pd-NZVI, and this approach likely results in a weaker binding of the CMC to the NZVI.[15] Our previous work also shows that covalent binding of CMC (rather than physisorption) during NZVI synthesis is a better approach to creating stable NZVI suspensions.[21] For magnetite nanoparticles, Hu et al.[40] demonstrated a significant shift in the CCC from 23.8 mM (in the absence of humic acid) to 125.5 mM (in the presence of 20 mg/L humic acid) while monitoring the aggregation kinetics as a function of the NaCl concentration (pH 9.8). These researchers reported $\alpha_{pp} \approx 0.002$ at 10 mM NaCl in the presence of 20 mg/L humic acid, which is nearly 1 order of magnitude lower compared to that of an uncoated magnetite particle, indicating a significantly higher stability in the aqueous environment. Likewise, Chen et al.[41] investigated the aggregation behavior of bare and alginate-coated hematite nanoparticles as a function of the NaCl concentration; the coated particle was found to be stable at lower solution IS, and the CCC was ~180 mM NaCl, which is much greater than the CCC of the bare hematite (~20 mM NaCl). The result clearly indicates heightened stability associated with alginate coating.

Careful inspection of the fitted stability curves (Figure 1b−d) determined by fitting eq 2 to the experimental data reveals two marked features. First, the slope in the unfavorable aggregation regime is an indication of the sensitivity of the particle suspension to changes in the solution IS. With a flatter slope (i.e., $\beta = 0.8$), the aggregation behavior of bare Pd-NZVI is less sensitive to the change in the solution IS compared to that of CMC-coated Pd-NZVI (β = 2.3) (Figure 1b). Here, the intrinsic aggregation rate of the bare particle likely supersedes the aggregation potential created with the addition of salt. This observation is consistent with the trend in EPM as a function of the IS (Figure S2, Supporting Information). Moreover, the steeper slope (β = 2.45) for SF-coated particles compared to SP treatment (β = 1.2) (Figure 1d) infers a greater sensitivity of

dx.doi.org/10.1021/es402619v | Environ. Sci. Technol. XXXX, XXX, XXX−XXX

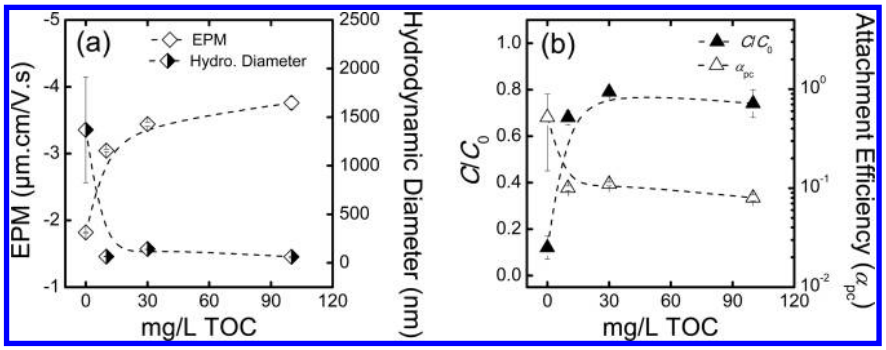

Figure 3. (a) Variation in electrophoretic mobility (EPM) and DLS-measured hydrodynamic diameter of Pd-NZVI as a function of the JBR215 rhamnolipid concentration at 10 mM $NaHCO_3$. The particle-collector attachment efficiency (α_{pc}) calculated using the TE correlation is also included in the figure. The dashed lines are included to guide the eye.

the former to the change in the solution IS. Interestingly, both JBR215-coated Pd-NZVI and R95-coated Pd-NZVI have similar slopes (β = 2.4) and are consistent with the trend of reported EPM behavior (Figure S2a). The second marked feature of the fitted stability curves is the horizontal shift, whereby a shift toward the left (to lower solution IS) is an indication of a less stable suspension. The results show that bare Pd-NZVI is less stable than CMC-coated Pd-NZVI, JBR215-coated Pd-NZVI is less stable than R95-coated Pd-NZVI, and SP-coated Pd-NZVI is less stable than SF-coated Pd-NZVI (Figure 1b–d). Overall, the stability (based on CCC) ranks in the following order: R95 rhamnolipid-coated > CMC-coated > SF-coated > SP-coated ≈ JBR215 rhamnolipid-coated > bare.

The temporal evolution of the PSDs was also observed and confirmed the stabilizing effect of select surface modifiers as well as the sensitivity of the suspensions to the change in the solution IS (Figures S5–S7, Supporting Information). As expected, the bare Pd-NZVI is unstable even at low IS (10 mM) as seen by a considerable shift of the PSD to larger particle diameters at both 10 and 300 mM (Figure S5a,b). At 10 mM, CMC-coated Pd-NZVI is stable; i.e., nearly identical PSDs are obtained at both 5 and 45 min (Figure S5c). However, the increase in the solution IS (to 300 mM) induces significant aggregation as depicted by the marked temporal shift of the PSD toward larger particle sizes (Figure S5d). The temporal change of the PSDs for JBR215- and R95-coated Pd-NZVI is presented in Figure S6. Although both particle suspensions are relatively stable at 10 mM IS, JBR215-coated particles result in a broader PSD compared to the relatively narrow PSD for R95-coated particles (Figure S6a,c). An increase in the solution IS to 300 mM induces significant aggregation as depicted by the marked temporal shift of the PSDs (Figure S6b,d). Similar behavior was observed for SF- and SP-coated Pd-NZVI, i.e., a nominal temporal change in PSDs at 10 mM and a marked shift toward larger sizes at 300 mM (Figure S7). Nevertheless, it is interesting to note that, at 10 mM, SF yields a more stable suspension than SP as seen by the relatively narrow and smaller sized PSD (Figure S7a,c). Phenrat et al.[14] also used DLS-measured PSDs to study NZVI aggregation kinetics. These researchers reported a considerable temporal shift of the PSDs toward larger particle size for bare NZVI in contrast to poly(styrenesulfonate)-stabilized NZVI, whose PSD did not change over time.

Deposition Kinetics under an Unfavorable Aggregation Regime. In the discussion of the Pd-NZVI aggregation kinetics, the stabilizing effect of selected surface modifiers and the role of the solution IS were highlighted. To assess the transport potential of coated Pd-NZVI at more stable conditions (i.e., when $\alpha_{pp} \ll 1$), a series of column experiments were conducted at 10 mM $NaHCO_3$. The measured particle breakthrough curves plotted as the normalized effluent particle concentration (C/C_0) as a function of PVs are presented in Figure 2a. As expected, the mobility of bare Pd-NZVI in the quartz sand is very limited ($C/C_0 < 0.10$). Visual inspection of the packed glass column revealed that the majority of the bare particles were entrapped in the upper 1–2 cm of the column. In contrast, the mobility of surface-modified Pd-NZVI is dramatically enhanced, and C/C_0 values range between 75% and 90% (Figure 2a). Physical filtration (i.e., straining) may have contributed to the retention of bare Pd-NZVI, which is supported by a marked reduction in the measured effluent particle hydrodynamic diameter (220 nm) in contrast to the predicted mean aggregate size at the column effluent (2389 nm, calculated using eq 3) and the actual measured average diameter of particles in the influent suspension (1370 nm) (Table 1). However, for coated Pd-NZVI, the average hydrodynamic diameters of the influent and effluent (both measured and predicted) nanoparticle suspensions do not exhibit such differences. Indeed, due to the considerably smaller size of coated Pd-NZVI particles, retention by physical straining is less likely in the quartz sand.[42] Electrosteric stabilization likely contributes to the observed enhanced transport of the surface-modified Pd-NZVI. Additionally, preconditioning of the packed column with the background electrolyte of interest (with surface modifier) could also contribute to the observed higher elution whereby the favorable deposition sites can be masked by the adsorbed negatively charged stabilizing surface modifiers.

The likelihood of particle attachment onto the sand surface is inferred by calculating the particle–collector attachment efficiency (α_{pc}) and deposition rate coefficient (k_d) (Figure 2c; Figure S8, Supporting Information). At 10 mM IS, the α_{pc} value for bare Pd-NZVI is ~0.5, which is notably higher than the calculated α_{pc} for coated Pd-NZVI, whose values range between 0.05 and 0.14. Naturally, similar trends were observed in the calculated deposition rate coefficient (k_d); the coated Pd-NZVI displays a substantially lower deposition rate (0.001–0.002 s^{-1}) compared to bare Pd-NZVI (0.008 s^{-1}) (Figure S8). In general, with moderate surface modification, α_{pc} can be reduced by approximately 1 order of magnitude. α_{pc} is a useful parameter to predict nanoparticle transport potential in subsurface environments, and hence, most of the selected surface modifiers seem to be promising for enhancing Pd-NZVI

dx.doi.org/10.1021/es402619v | Environ. Sci. Technol. XXXX, XXX, XXX–XXX

mobility. Interestingly, the extent of adsorption of the different surface modifiers onto the Pd-NZVI surface (R95 > JBR215 > SM > SF > CMC > SP; Figure S3, Supporting Information) correlates both with transport (Figure 2b) and stability (Figure 1b–d) plots and thereby implies that greater adsorbed mass of the stabilizing molecules leads to enhanced particle stability and mobility.

Given the relatively small measured particle sizes and low calculated α_{pc} values at 10 mM IS, the two rhamnolipids used herein are of particular interest as natural stabilizing agents for Pd-NZVI (Table 1 and Figure 2c). The JBR215 rhamnolipid is significantly more cost-effective in bulk quantities relevant for field applications than the R95 product and was therefore selected for more in depth investigation of its effect on nanoparticle size, EPM, and transport potential over a broad range of rhamnolipid concentrations (0, 10, 30, and 100 mg/L TOC). Interestingly, only 10 mg/L JBR215 rhamnolipid appears to be sufficient to stabilize the bare Pd-NZVI and concurrently enhance its transport (Figure 3).

Deposition Kinetics under a Favorable Aggregation Regime. In an effort to assess the transport potential of surface-modified Pd-NZVI under a less stable condition (i.e., when $\alpha_{pp} \approx 1$), a series of column experiments were conducted at 300 mM $NaHCO_3$. The measured particle breakthrough curves are presented in Figure 2b. Overall, an increase in salt concentration from 10 to 300 mM $NaHCO_3$ results in increased Pd-NZVI retention. While the elution of bare and CMC- and SP-coated Pd-NZVI is negligible ($C/C_0 < 0.1$), we observe higher elution for SM-coated ($C/C_0 \approx 0.29$) and SF-coated ($C/C_0 \approx 0.23$) Pd-NZVI, and most interestingly, the elution of both JBR215-coated ($C/C_0 \approx 0.49$) and R95-coated ($C/C_0 \approx 0.68$) Pd-NZVI is dramatically higher. As seen from Figure 2a, for coated Pd-NZVI at 10 mM, there is a limited range in the steady-state elution concentration among the different coatings (C/C_0 ranged between 0.75 and 0.90); in contrast, at 300 mM, the difference is more significant (C/C_0 ranged between 0.02 and 0.68).

At 300 mM, the α_{pc} values are relatively higher compared to those in the corresponding experiment at 10 mM for each treatment (Figure 2c). For coated Pd-NZVI, the EPM generally becomes less negative with an increase in the salt concentration (Figure S2, Supporting Information, and Table 1). Therefore, the observed deposition behavior qualitatively follows the trend predicted by the DLVO theory.

A careful inspection of Table 1 also reveals a marked difference in influent and effluent hydrodynamic diameters for experiments conducted at 300 mM. Overall, the measured effluent particle size is smaller than the influent size at 300 mM (except for the SM coating). These data suggest that the preferential retention of larger aggregates occurs in the granular material and thereby implies that physical straining partially contributes to the observed increased retention.

At this higher salt concentration (300 mM), the transport of JBR215- and R95-coated Pd-NZVI is higher than that of soy- and CMC-coated Pd-NZVI; however, there is a marked difference in the shape of the particle breakthrough curves. For JBR215-coated Pd-NZVI, the deposition behavior exhibits a shape characteristic of "ripening", whereby the approaching particles deposit on the surface of already deposited particles, resulting in a temporal decrease in the effluent particle concentration.[43,44] In contrast, R95-coated Pd-NZVI exhibits a "blocking" type of deposition behavior whereby potential deposition sites for the approaching particles are blocked by previously deposited particles. The lower α_{pc} values for JBR215-coated (0.24) and R95-coated (0.12) Pd-NZVI infer higher transport potential of these particles even at the high IS (300 mM) condition. While the charge that confers some electrostatic stabilization to the rhamnolipid-coated Pd-NZVI is attributed to the carboxyl group, the presence of a larger headgroup with dirhamnolipid has been reported as a contributing factor for the steric hindrance.[45] At 300 mM, although the electrostatic charges are effectively screened (much lower absolute EPM values; Figure S2, Supporting Information), the steric components are likely not completely collapsed.

■ ENVIRONMENTAL IMPLICATIONS

The success of Pd-NZVI-based in situ site remediation largely depends on the mobility of injected nanoparticles to reach the contaminant of interest. A large body of literature has emphasized stabilization of nonpalladized NZVI through a surface modification approach. Given the substantially enhanced reactivity of Pd-NZVI, it is of interest to assess the transport potential of these more reactive nanoparticles in a model groundwater environment. We have shown rhamnolipid biosurfactants (biological origin) and soy protein (food-grade origin) as promising stabilizers that can reduce Pd-NZVI aggregation and concurrently enhance its mobility. These nontoxic and biodegradable surface modifiers may have less impact on the environment and are effective at much lower concentrations than other polymers commonly used for NZVI stabilization. For instance, in a few of the previous studies, the polymer TOC to NZVI mass ratios were 0.17,[46] 0.83,[25] and 0.99,[13] whereas the TOC to NZVI mass ratio for JBR215 rhamnolipid used in this study is 0.07.

Our results show that selected surface modifiers have varied stabilizing efficiencies. Both JBR215 and R95 rhamnolipids seem promising to render Pd-NZVI mobile in a wide range of groundwater IS, whereas SP-coated Pd-NZVI stability and transport seem fairly comparable to those of CMC-coated Pd-NZVI. Therefore, to better emplace these reactive particles in the targeted contaminated zone, a site-specific design to address the subsurface complexities is necessary. Additionally, further research is needed to systematically investigate the mobility of these particles in more environmentally relevant media (e.g., in the presence of biological or organic films on collector surfaces). Ideally, the Pd-NZVI mobility should be just enough to reach the contaminant as nanoparticle transport beyond the contaminant of interest is generally undesirable.

■ ASSOCIATED CONTENT

Ⓢ Supporting Information

Details on the surface modifiers, measured interfacial tension of rhamnolipids, adsorbed concentration of surface modifiers on the Pd-NZVI surface, selected TEM images, representative PSDs as a function of time, and calculated deposition rate coefficients. This material is available free of charge via the Internet at http://pubs.acs.org.

■ AUTHOR INFORMATION

Corresponding Author

*Phone: 514-398-2999. Fax: 514-398-6678. E-mail: nathalie.tufenkji@mcgill.ca.

Notes

The authors declare no competing financial interest.

■ ACKNOWLEDGMENTS

This research was supported by the Natural Sciences and Engineering Research Council of Canada (NSERC Strategic Grant 365253), Golder Associates Inc., the Fonds Québecois de la Recherche sur la Nature et les Technologies (FQRNT), Environment Canada, the Ministère du Développement Économique, Innovation et Exportation (MDEIE), a McGill Engineering Doctoral Award (MEDA) to M.B., and the CRC program. We thank Che O'May for assistance with manuscript editing.

■ REFERENCES

(1) Karn, B.; Kuiken, T.; Otto, M. Nanotechnology and *in situ* remediation: A review of the benefits and potential risks. *Environ. Health Perspect.* **2009**, *117*, (12).

(2) Zhang, W.-x. Nanoscale iron particles for environmental remediation: An overview. *J. Nanopart. Res.* **2003**, *5* (3), 323−332.

(3) He, F.; Zhao, D.; Liu, J.; Roberts, C. B. Stabilization of Fe-Pd nanoparticles with sodium carboxymethyl cellulose for enhanced transport and dechlorination of trichloroethylene in soil and groundwater. *Ind. Eng. Chem. Res.* **2006**, *46* (1), 29−34.

(4) Saleh, N.; Sirk, K.; Liu, Y.; Phenrat, T.; Dufour, B.; Matyjaszewski, K.; Tilton, R. D.; Lowry, G. V., Surface Modifications enhance nanoiron transport and NAPL targeting in saturated porous media. *Environ. Eng. Sci.* **2007**, *24*, (1), 45−57.

(5) Phenrat, T.; Saleh, N.; Sirk, K.; Tilton, R. D.; Lowry, G. V. Aggregation and sedimentation of aqueous nanoscale zerovalent iron dispersions. *Environ. Sci. Technol.* **2006**, *41* (1), 284−290.

(6) Lowry, G. V.; Gregory, K. B.; Apte, S. C.; Lead, J. R. Transformations of nanomaterials in the environment. *Environ. Sci. Technol.* **2012**, *46* (13), 6893−6899.

(7) de Gennes, P. G. Polymers at an interface; a simplified view. *Adv. Colloid Interface Sci.* **1987**, *27* (3−4), 189−209.

(8) Wiesner, M. R.; Bottero, J.-Y. *Environmental Nanotechnology: Applications and Impacts of Nanomaterials*; The McGraw-Hill Companies: New York, 2007.

(9) Verwey, E.; Overbeek, J. T. G. *Theory of the Stability of Lyophobic Colloids*; Elsevier: Amsterdam, 1948.

(10) Derjaguin, B.; Landau, L. Theory of the stability of strongly charged lyophobic sols and of the adhesion of strongly charged particles in solution of electrolytes. *Acta Physicochim. URSS* **1941**, *14*, 633−662.

(11) Elimelech, M.; Gregory, J.; Jia, X.; Williams, R. *Particle Deposition and Aggregation: Measurement, Modelling and Simulation*; Butterworth-Heinemann: Boston, MA, 1995.

(12) Petosa, A. R.; Jaisi, D. P.; Quevedo, I. R.; Elimelech, M.; Tufenkji, N. Aggregation and deposition of engineered nanomaterials in aquatic environments: Role of physicochemical interactions. *Environ. Sci. Technol.* **2010**, *44* (17), 6532−6549.

(13) Tiraferri, A.; Chen, K. L.; Sethi, R.; Elimelech, M. Reduced aggregation and sedimentation of zero-valent iron nanoparticles in the presence of guar gum. *J. Colloid Interface Sci.* **2008**, *324* (1−2), 71−79.

(14) Phenrat, T.; Saleh, N.; Sirk, K.; Kim, H.-J.; Tilton, R.; Lowry, G. Stabilization of aqueous nanoscale zerovalent iron dispersions by anionic polyelectrolytes: Adsorbed anionic polyelectrolyte layer properties and their effect on aggregation and sedimentation. *J. Nanopart. Res.* **2008**, *10* (5), 795−814.

(15) Cirtiu, C. M.; Raychoudhury, T.; Ghoshal, S.; Moores, A. Systematic comparison of the size, surface characteristics and colloidal stability of zero valent iron nanoparticles pre- and post-grafted with common polymers. *Colloids Surf., A* **2011**, *390* (1−3), 95−104.

(16) Krajangpan, S.; Kalita, H.; Chisholm, B. J.; Bezbaruah, A. N. Iron nanoparticles coated with amphiphilic polysiloxane graft copolymers: Dispersibility and contaminant treatability. *Environ. Sci. Technol.* **2012**, *46* (18), 10130−10136.

(17) Tiraferri, A.; Sethi, R. Enhanced transport of zerovalent iron nanoparticles in saturated porous media by guar gum. *J. Nanopart. Res.* **2009**, *11* (3), 635−645.

(18) Saleh, N.; Kim, H.-J.; Phenrat, T.; Matyjaszewski, K.; Tilton, R. D.; Lowry, G. V. Ionic strength and composition affect the mobility of surface-modified Fe^0 nanoparticles in water-saturated sand columns. *Environ. Sci. Technol.* **2008**, *42* (9), 3349−3355.

(19) Raychoudhury, T.; Naja, G.; Ghoshal, S. Assessment of transport of two polyelectrolyte-stabilized zero-valent iron nanoparticles in porous media. *J. Contam. Hydrol.* **2010**, *118* (3−4), 143−151.

(20) Vecchia, E. D.; Luna, M.; Sethi, R. Transport in porous media of highly concentrated iron micro- and nanoparticles in the presence of xanthan gum. *Environ. Sci. Technol.* **2009**, *43* (23), 8942−8947.

(21) Fatisson, J.; Ghoshal, S.; Tufenkji, N. Deposition of carboxymethylcellulose-coated zero-valent iron nanoparticles onto silica: roles of solution chemistry and organic molecules. *Langmuir* **2010**, *26* (15), 12832−12840.

(22) Schrick, B.; Hydutsky, B. W.; Blough, J. L.; Mallouk, T. E. Delivery vehicles for zerovalent metal nanoparticles in soil and groundwater. *Chem. Mater.* **2004**, *16* (11), 2187−2193.

(23) Saleh, N.; Phenrat, T.; Sirk, K.; Dufour, B.; Ok, J.; Sarbu, T.; Matyjaszewski, K.; Tilton, R. D.; Lowry, G. V. Adsorbed triblock copolymers deliver reactive iron nanoparticles to the oil/water interface. *Nano Lett.* **2005**, *5* (12), 2489−2494.

(24) Kanel, S.; Nepal, D.; Manning, B.; Choi, H. Transport of surface-modified iron nanoparticle in porous media and application to arsenic(III) remediation. *J. Nanopart. Res.* **2007**, *9* (5), 725−735.

(25) Raychoudhury, T.; Tufenkji, N.; Ghoshal, S. Aggregation and deposition kinetics of carboxymethyl cellulose-modified zero-valent iron nanoparticles in porous media. *Water Res.* **2012**, *46* (6), 1735−1744.

(26) He, F.; Zhao, D. Preparation and characterization of a new class of starch-stabilized bimetallic nanoparticles for degradation of chlorinated hydrocarbons in water. *Environ. Sci. Technol.* **2005**, *39* (9), 3314−3320.

(27) Jiemvarangkul, P.; Zhang, W.-x.; Lien, H.-L. Enhanced transport of polyelectrolyte stabilized nanoscale zero-valent iron (nZVI) in porous media. *Chem. Eng. J.* **2011**, *170* (2−3), 482−491.

(28) Mulligan, C. N. Recent advances in the environmental applications of biosurfactants. *Curr. Opin. Colloid Interface Sci.* **2009**, *14* (5), 372−378.

(29) Fan, G.; Cang, L.; Qin, W.; Zhou, C.; Gomes, H. I.; Zhou, D. Surfactants-enhanced electrokinetic transport of xanthan gum stabilized nanoPd/Fe for the remediation of PCBs contaminated soils. *Sep. Purif. Technol.* **2013**, *114*, 64−72.

(30) Lai, C. C.; Huang, Y. C.; Wei, Y. H.; Chang, J. S. Biosurfactant-enhanced removal of total petroleum hydrocarbons from contaminated soil. *J. Hazard. Mater.* **2009**, *167* (1−3), 609−614.

(31) Juwarkar, A. A.; Nair, A.; Dubey, K. V.; Singh, S. K.; Devotta, S. Biosurfactant technology for remediation of cadmium and lead contaminated soils. *Chemosphere* **2007**, *68* (10), 1996−2002.

(32) Johnson, R. L.; Johnson, G. O. B.; Nurmi, J. T.; Tratnyek, P. G. Natural organic matter enhanced mobility of nano zerovalent iron. *Environ. Sci. Technol.* **2009**, *43* (14), 5455−5460.

(33) Grittini, C.; Malcomson, M.; Fernando, Q.; Korte, N. Rapid dechlorination of polychlorinated biphenyls on the surface of a Pd/Fe bimetallic system. *Environ. Sci. Technol.* **2002**, *29* (11), 2898−2900.

(34) Lowry, G. V.; Reinhard, M. Hydrodehalogenation of 1- to 3-carbon halogenated organic compounds in water using a palladium catalyst and hydrogen gas. *Environ. Sci. Technol.* **1999**, *33* (11), 1905−1910.

(35) Sakulchaicharoen, N.; O'Carroll, D. M.; Herrera, J. E. Enhanced stability and dechlorination activity of pre-synthesis stabilized nanoscale FePd particles. *J. Contam. Hydrol.* **2010**, *118* (3−4), 117−127.

(36) Grolimund, D.; Elimelech, M.; Borkovec, M. Aggregation and deposition kinetics of mobile colloidal particles in natural porous media. *Colloids Surf., A* **2001**, *191* (1−2), 179−188.

(37) Pelley, A. J.; Tufenkji, N. Effect of particle size and natural organic matter on the migration of nano- and microscale latex particles in saturated porous media. *J. Colloid Interface Sci.* **2008**, *321* (1), 74−83.
(38) Yao, K.-M.; Habibian, M. T.; O'Melia, C. R. Water and waste water filtration. Concepts and applications. *Environ. Sci. Technol.* **1971**, *5* (11), 1105−1112.
(39) Tufenkji, N.; Elimelech, M. Correlation equation for predicting single-collector efficiency in physicochemical filtration in saturated porous media. *Environ. Sci. Technol.* **2004**, *38* (2), 529−536.
(40) Hu, J.-D.; Zevi, Y.; Kou, X.-M.; Xiao, J.; Wang, X.-J.; Jin, Y. Effect of dissolved organic matter on the stability of magnetite nanoparticles under different pH and ionic strength conditions. *Sci. Total Environ.* **2010**, *408* (16), 3477−3489.
(41) Chen, K. L.; Mylon, S. E.; Elimelech, M. Aggregation kinetics of alginate-coated hematite nanoparticles in monovalent and divalent electrolytes. *Environ. Sci. Technol.* **2006**, *40* (5), 1516−1523.
(42) Tufenkji, N.; Miller, G. F.; Ryan, J. N.; Harvey, R. W.; Elimelech, M. Transport of *Cryptosporidium* oocysts in porous media: Role of straining and physicochemical filtration. *Environ. Sci. Technol.* **2004**, *38* (22), 5932−5938.
(43) Kuhnen, F.; Barmettler, K.; Bhattacharjee, S.; Elimelech, M.; Kretzschmar, R. Transport of iron oxide colloids in packed quartz sand media: Monolayer and multilayer deposition. *J. Colloid Interface Sci.* **2000**, *231* (1), 32−41.
(44) Tufenkji, N.; Redman, J. A.; Elimelech, M. Interpreting deposition patterns of microbial particles in laboratory-scale column experiments. *Environ. Sci. Technol.* **2003**, *37* (3), 616−623.
(45) Cohen, R.; Ozdemir, G.; Exerowa, D. Free thin liquid films (foam films) from rhamnolipids: Type of the film and stability. *Colloids Surf., B* **2003**, *29* (2−3), 197−204.
(46) Phenrat, T.; Kim, H.-J.; Fagerlund, F.; Illangasekare, T.; Tilton, R. D.; Lowry, G. V. Particle size distribution, concentration, and magnetic attraction affect transport of polymer-modified Fe^0 nanoparticles in sand columns. *Environ. Sci. Technol.* **2009**, *43* (13), 5079−5085.